SUPERFAST ELECTROKINETICS

By

Mehrnaz Rouhi Youssefi

A thesis submitted to the

Graduate School-New Brunswick

Rutgers, The State University of New Jersey

In partial fulfillment of the requirements

For the degree of

Master of Science

Graduate Program in Mechanical and Aerospace Engineering

Written under the direction of

Dr. Francisco J. Diez

And approved by

_____

_____

_____

New Brunswick, New Jersey

MAY 2014

ABSTRACT OF THE THESIS

Superfast Electrokinetics

by MEHRNAZ ROUHI YOUSSEFI

Thesis Director:

Dr F. Javier Diez-Garias

Electrokinetics provides one of the most plausible alternatives to mechanical pumping in microfluidics. Among its advantages are small volume, fundamental simplicity, overall low mass, and cost efficiency. Our work describes an experimental investigation of the superfast electrokinetics and represents the first attempts to obtain orders of magnitude higher velocities in microchannels. The significance of superfast electrokinetics is to design efficient micro pumps, space actuators, and sea gliders. The influence of applied electric field on both fluid and particle mobilities was quantified at high Peclet numbers using particle image velocimetry and flow rate measurements, simultaneously. The experiments are conducted at very short PDMS microchannels using polystyrene tracer particles and deionized water as the background flow. Electroosmotic slip velocities as large as 3 m/sec are obtained by applying very high electric fields. Classical linear electrokinetic theories cannot explain the experimental behavior of microfluidic systems in these extreme experimental conditions. The increasing field strength causes a rise in the density of ion fluxes at particle surfaces which leads to the

deviation of the electrical double layer from the equilibrium state as a result of a local rearrangement in the electrolyte concentration and a potential drop. A secondary diffuse layer of counterions (space charge) is induced outside the primary electrical double layer because of concentration polarization. The nonlinearity associated with the effect of the electric field on the resulting induced charge is consistent with the obtained experimental data. Features of nonlinear electrophoresis are crucial in control, separation and manipulation of colloidal particles.

Contents

1. Introduction

Electrophoresis arises when charged colloidal particles are subjected to an outer electric field, and under the effect of this field the particles begin to move with respect to fluid. At low electric field strength, the electrophoretic velocity changes [1, 2] linearly with the electric field and is described by the Helmholtz-Smoluchowski equation. However, as the field strength is enhanced, this dependence becomes nonlinear.

The increasing field strength causes a rise in the density of ion fluxes at particle surfaces [3] which leads to the deviation of the electrical double layer (EDL) from the equilibrium state as a result of a local rearrangement in the electrolyte concentration and a potential drop [3, 4] . This change in the electrolyte concentration depends on the electromigration, diffusion, and convection processes that develop near the particle surface [3, 6].

Nonlinear electrokinetic models that were predicted for conducting particles have been experimentally studied in detail, while, in the case of nonconducting particles, theoretical models [10–13] of polarization processes and relevant nonlinear electro kinetic phenomena have only been confirmed by scarce experimental data using the so called aperiodic electrophoresis measurements [14–19]. Our measurements are performed using non conducting particles to fill the gap in previous experimental data and investigate nonlinearity of electrophoresis at very high electric fields.

Nonlinear electrokinetic phenomena can be categorized by the introduction of two dimensionless parameters: Dukhin number which determines the ratio

between the conductivity of particle surface and bulk conductivity [6–9], and Peclet number which describes the balance between convective and diffusive processes near the particle surface. In order to simplify the study of polarization processes and non-equilibrium DL phenomena, the cases of small, intermediate, and large Peclet numbers will be considered separately in the following discussion.

Classical nonlinear models suggest that at low Peclet numbers the expression describing electrophoresis velocity is proportional to the cubed strength of an applied electric field which is associated with a low polarization charge generated in the EDL and outside it [6, 20].

The theoretical description of nonlinear electrophoresis at large Peclet numbers (Pe $\geq$ 3) was considered for two limiting cases of weak [7, 19, 21] and strong [8, 10–11] concentration polarization. In these limiting cases, the electrolyte concentration in the convective–diffuse layer at the external boundary of the EDL in the particle side that accepts counterions decrease by 20–30% or drops to almost zero, respectively. In the case of the weak concentration polarization, the nonlinear component of the velocity is proportional to $E^{3/2}$ [12, 22]. Because of the complexity of the problem in question, in the case of strong concentration polarization, the analytical solution was only obtained for the velocity of electroosmosis .They suggest that on the particle side that accepts counterions, the electroosmosis velocity rises in proportion to E^2. According to a numerical calculation [8] the electrophoresis increases with electric field strength somewhat more slowly than $E^{3/2}$.

In the previous studies peclet number did not exceeded 10. Here we consider the case of superfast electrophoresis ($Pe \geq 100$) resulted from large electric fields and the corresponding concentration polarization associated with it. Understanding the processes behind superfast electrophoresis plays a significant role in the development of new technologies, for instance, separation of matters in electrochromatography, sorting of particles by their sizes and electroconductivity, sample preparation, drug delivery, and others.

Another electrokinetic phenomenon of interest arises from the interface between an electrolyte solution and a polarizable surface such as the walls of a microchannel made of materials such as a variety of polymers or glass. The physics at this interface are known to create an electrical potential at a shear plane in the fluid very close to the wall which results in ion redistribution and formation of an EDL on the surface of the wall. The interaction of an applied outer electric field and the EDL gives rise to drag and movement of EDL and the surrounding fluid in the direction of the field. The flow generated in this way is known as electroosmosis and can be used to pump [24] and mix fluids at micron scales, where pressure-driven flows and inertial instabilities are suppressed by viscosity. A key objective of non-mechanical electroosmotic micro pumps is to fabricate a platform capable of generating high flow rates and thrusts, while maintaining a minimal weight and power consumption. In this study, we explore fastest electroosmotic flows which may be generated in microfluidic devices by applying high electric fields along very short microchannels.

2. Theory

The theory of the electrokinetic phenomena has always been developed traditionally on the basis of the concept of complete equilibrium of the double layer. At low electric fields the assumption of complete equilibrium of the double layer can be considered valid, and the particle velocity linearly depends on E, and is described by the Smoluchowski equation as follows:

$$V_{ep} = \frac{\varepsilon_r \varepsilon_0}{\eta} \zeta_0 E \qquad (1)$$

However, the DL transforms from its equilibrium state into a non-equilibrium state under any effect causing internal ion flux, e.g. by applying an external electric field, particle sedimentation, and Brownian motion.

Figure 1 presents a comparison of the equilibrium and non-equilibrium DL[25]. An external electric field directed from left to right displaces the counter ions of DL to the right. Hence, the Dl becomes anti symmetric and a field-induced dipole is generated.

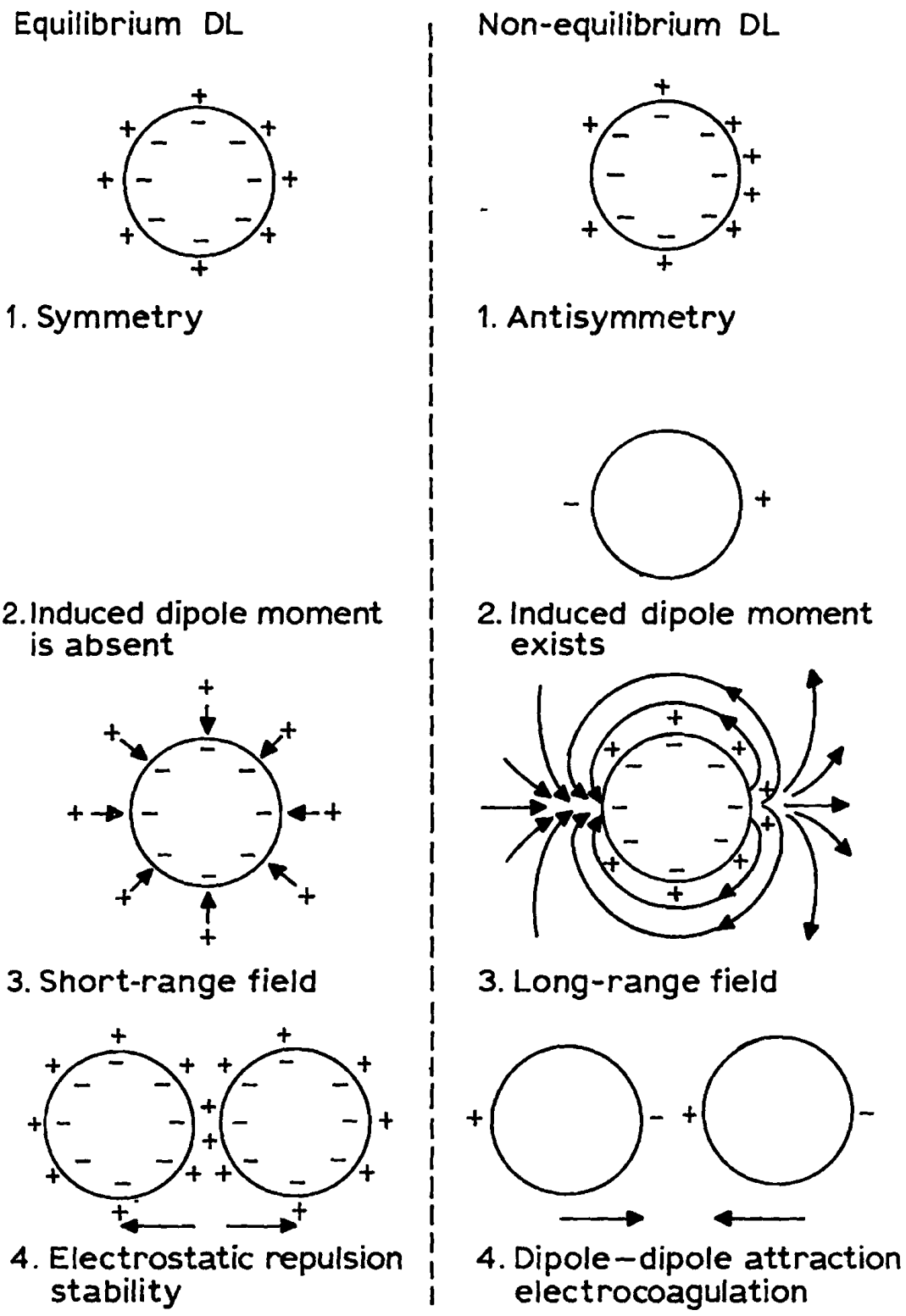

Figure 1. A comparison of the characteristics of the equilibrium and non-equilibrium DL[25]

The electric filed of the symmetric DL is short ranged, and does not reach beyond its limits, whereas the electric field lines of induced field dipole moment in the non-equilibrium DL originate in the right hemisphere and terminate on the left as depicted in Fig. 1, hence generating a long-range potential field and a conjugated concentration field[1, 2].

Fig. 2 illustrates the generation of this concentration field. DL deviation from equilibrium is accompanied by the emergence of the hydrodynamic fields beyond the DL limit known as secondary the diffusion layer in previous studies.

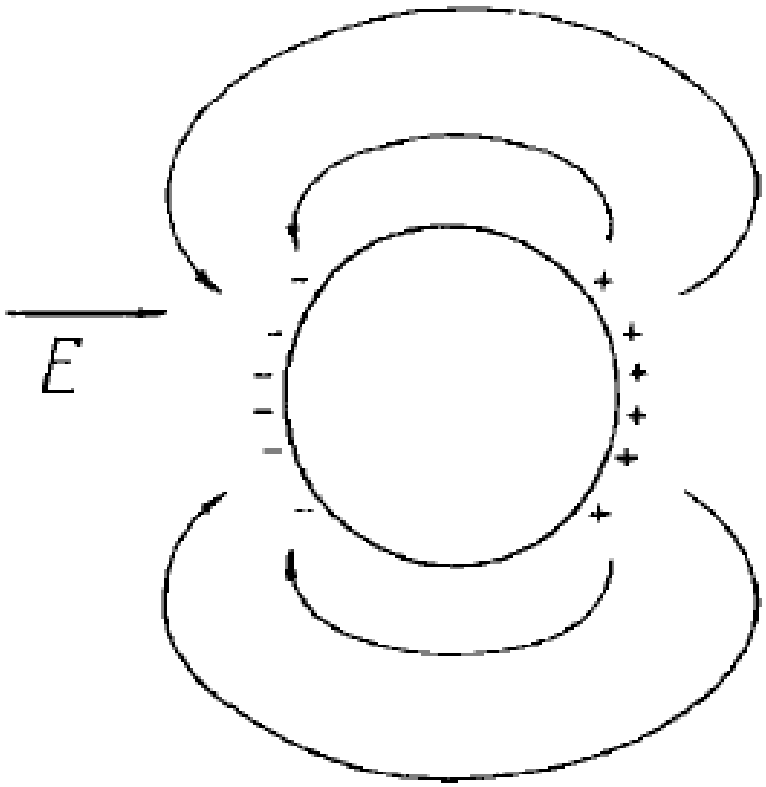

Figure 2. Illustration of the concentration polarization for a spherical particle[27]

As mentioned before, nonlinear electrokinetic phenomena that were predicted for conducting particles [28][29] have been experimentally studied in detail[30][31][32], while, in the case of nonconducting particles, theoretical models [3–12] of polarization processes and relevant nonlinear electro kinetic phenomena have only been confirmed by scarce experimental data using the so called aperiodic electrophoresis measurements [3, 4, 13– 16].

Nonlinear electrokinetic phenomena can be characterized by the introduction of two dimensionless parameters: Dukhin number which determines the ratio between surface and bulk conductance, and Peclet number which describes the balance between convection and diffusion processes.

$$Du = \frac{K^{\sigma}}{K_m a} \tag{2}$$

$$Pe = \frac{aU_{ef}}{D_{eff}} \tag{3}$$

At very small Dukhin numbers, the deviation from linear Smoluchowski is not appreciable. However, at $Du \gg 0.1$ the nonlinearity can become large. Fig.3 shows the possible values of Dukhin number in our experiments calculated according to its simplest expression when the stern and zeta potential coincide:

$$Du = \frac{2\sinh(\bar{\zeta}_0/2)}{\kappa a} \tag{4}$$

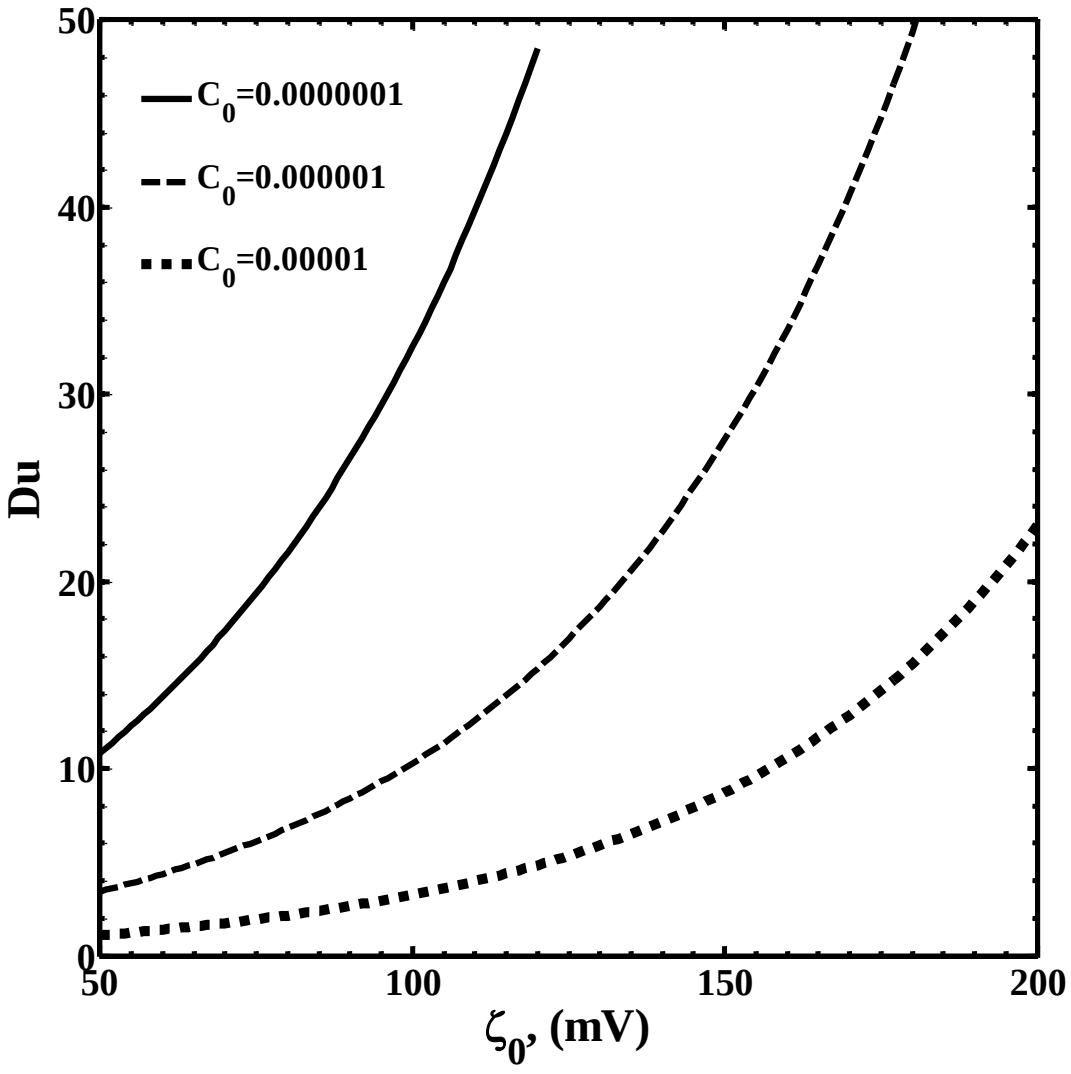

Figure 3. The dependence of Dukhin number on zeta potential for electrolyte concentrations of $\mathbf{c_0 = 10^{-7}, 10^{-6}, 10^{-5}}$

The degree of concentration polarization of the fluid around the particles and electrophoretic velocity also strongly depends on the Peclet number. Theoretical models have been developed for two limiting cases of low ($Pe < 1$) and high ($Pe \gg 1$) Peclet numbers. For the intermediate range $1 < Pe < 10$ no theory has been developed, but certain deviations from linear electrokinetic models is expected. Fig.4 illustrates the range of our Peclet numbers located in intermediate and very high Peclet numbers.

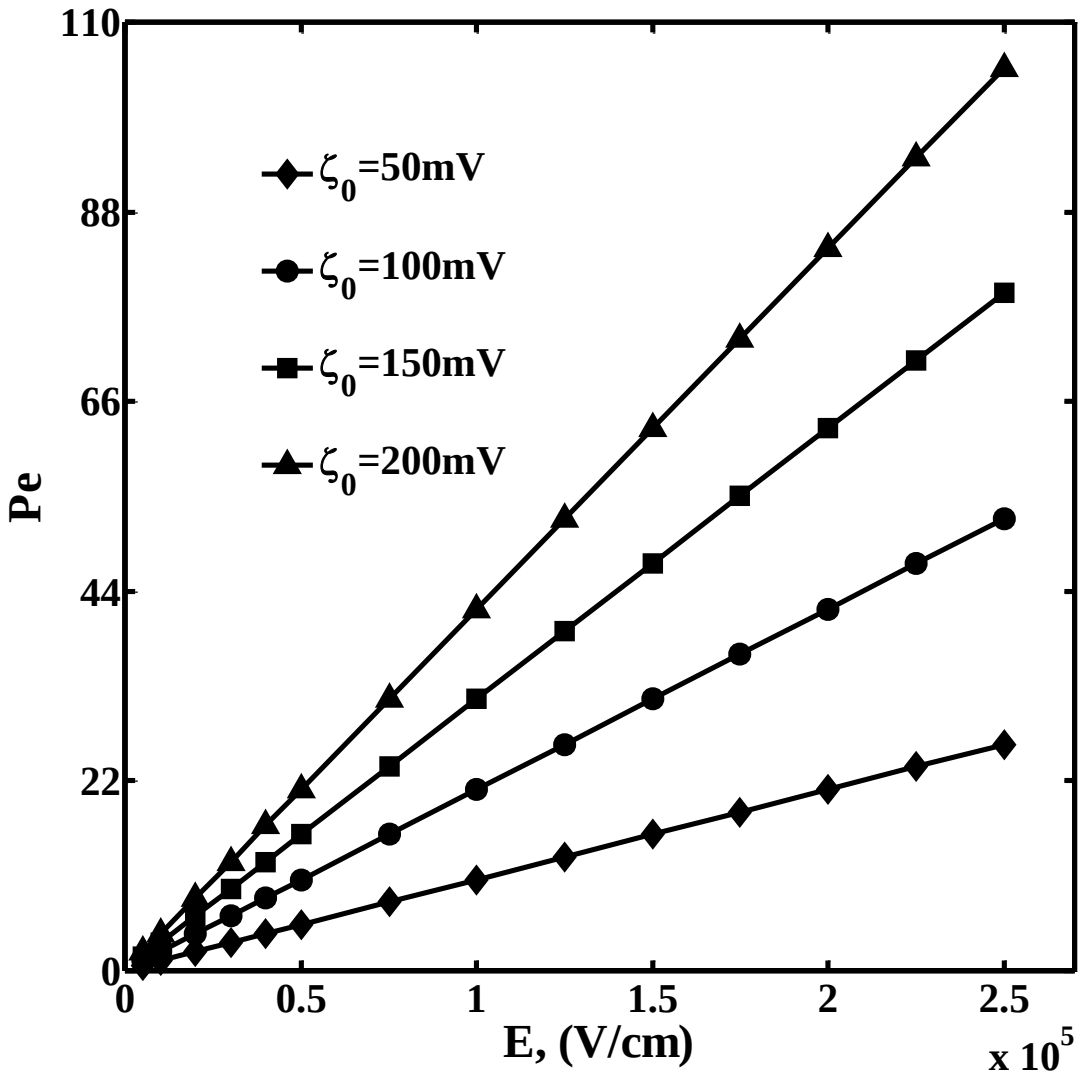

Figure 4. The dependence of the Peclet number calculated according to Smoluchowski's expression on electric field based on $\boldsymbol{\zeta_0 = 100, 150, 200}$ mV

In order to simplify the study of polarization processes and non-equilibrium DL phenomena, the cases of small and large Pe numbers will be considered separately in the following discussion.

2.1. Nonlinear electrophoresis at small Peclet numbers

The distribution of potential in a solution of an electrolyte around a spherical particle under the action of a homogenous electric field satisfies the equation:

$$E = -\nabla\varphi \tag{5}$$

Close to the particle, the potential distribution is perturbed due to the induced dipole and inhomogeneity in solution conductivity. The field induced dipole gives rise to concentration polarization field near the particle. The deviation of electrolyte concentration and electric potential provide the continuity of ion fluxes

$$\nabla . j^{\pm} = 0 \tag{6}$$

Where the ion flux density $j^{\pm}$ can be represented by the sum of three components caused by migration in the electric field, by diffusion, and by electroosmotic slip of the liquid (namely convection).If the Pe number is small compared with unity, then the impact of convection on the concentration field can be neglected and the ion flux density can be described as

$$j^{\pm} = \frac{-D^{\pm}c^{\pm}}{kT}\nabla\mu^{\pm} = -\frac{D^{\pm}c^{\pm}}{kT}(kT\nabla\ln(c) + z^{\pm}e\nabla\varphi) \tag{7}$$

Substituting Eq. (7) into (6), in the frame of the first approximation with respect to E, and neglecting the product among field induced values, one obtains:

$$\nabla^2\varphi = 0 \tag{8}$$

$$\nabla^2 c = 0 \tag{9}$$

Conservation of ions at the surface of particle can be written as:

$$j_r^{\pm}|_{r=a} = -\nabla.I_s^{\pm} = \nabla_s.\left(I_E^{\pm} + I_D^{\pm} + I_V^{\pm}\right) \tag{10}$$

For thin EDL, approximation of local equilibrium between EDL and the adjacent electrolyte requires that the ion electrochemical potentials to be independent of radial component and just vary with tangential component. The surface ion flows can be described as:

$$j_s^{\pm} = -\frac{D_s^{\pm}\Gamma_s^{\pm}}{kT}\left(\frac{\nabla_\theta c}{c_0} \pm z^{\pm}e\nabla_\theta\varphi\right)\Big|_{r=a} \tag{11}$$

where $D_s^{\pm}$ and $\Gamma_s^{\pm}$ are the surface densities and diffusion coefficient of ions in EDL respectively. Surface conductivity is defined based on these parameters as:

$$K^{\sigma} = \frac{(ez^{+})^2}{kT}D_s^{\pm}\Gamma_s^{+} + \frac{(ez^{-})^2}{kT}D_s^{-}\Gamma_s^{-} \tag{12}$$

The local deformation of the electric field vector lines is caused by the fact that the field of the generated particle dipole is added to the homogeneous electric

field. The extent of the vector line deformation and the resulting concentration polarization depends on electromigration, diffusion and convection processes in EDL and beyond it with their role being determined by the Dukhin number. The effect of Du on the field around a non-conducting (dielectric) spherical particle is sketched in Fig. 5.

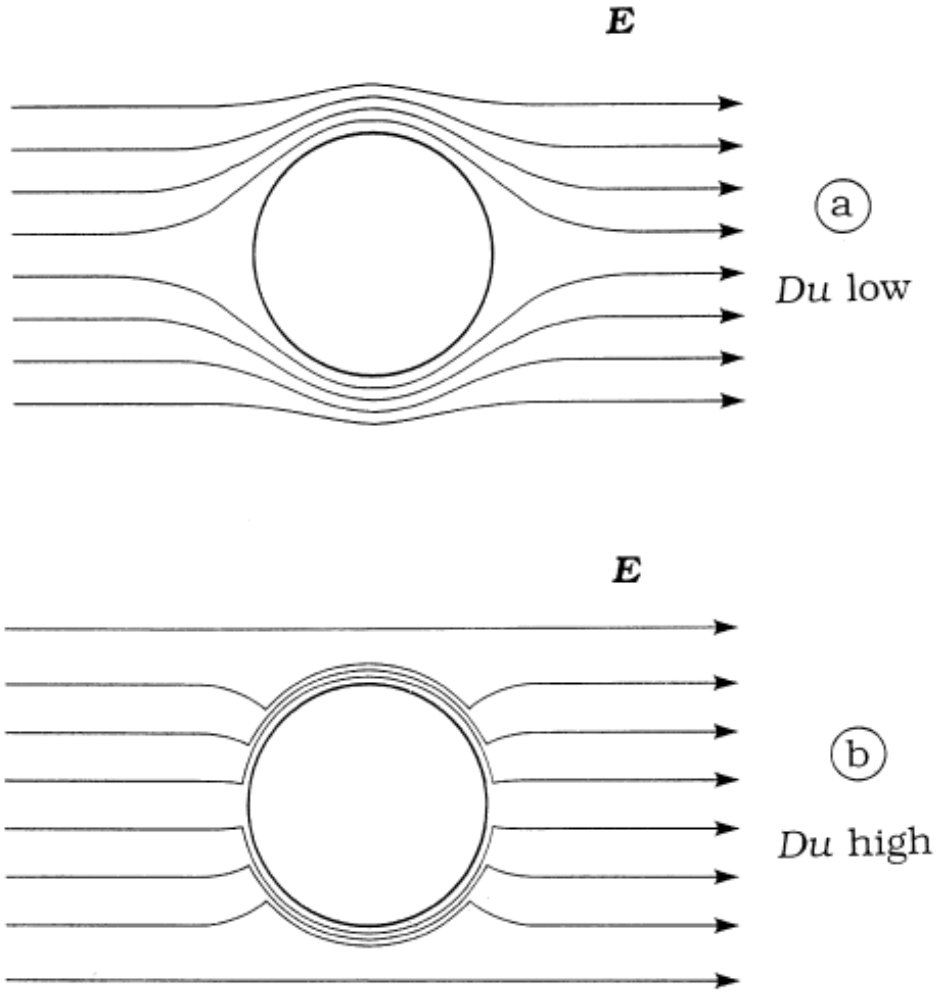

Figure 5. Dielectric particle in an external field; the role of Du[33]

If we neglect the surface flux of co-ions, convection especially for the case of high Dukhin numbers, we can rewrite Eq. (10) in the following form using Eqs. (7) and (11):

$$\frac{D^+c^+}{kT}\left(\frac{kT}{c_0}\nabla_r c + z^+e\nabla_r\varphi\right)\Big|_{r=a} = -\frac{K^\sigma}{(ez^+)^2}\nabla_s.\left(\frac{kT}{c_0}\nabla_\theta c + z^+e\nabla_\theta\varphi\right)\Big|_{r=a} \tag{13}$$

$$\left(\frac{kT}{c_0}\nabla_r c - z^-e\nabla_r\varphi\right)\Big|_{r=a} = 0 \tag{14}$$

Considering Eqs. (5), (8) and (9), the following form of the solution for potential and concentration fields is obtained:

$$\varphi(r,\theta) = -Ercos\theta + \frac{d_\varphi}{r^2}cos\theta \tag{15}$$

$$c(r,\theta) = c_0 + \frac{d_c}{r^2}cos\theta \tag{16}$$

The values of the field-induced electric dipole and concentration dipole can be obtained by substitution of Eqs. (15) and (16) into Eqs. (13) and (14). The solution of this system is:

$$d_{\varphi} = \frac{(2z^+ - z^-)Du - (z^+ + z^-)t^+}{2(Du + t^+)(z^+ + z^-)} E_0 a^3 \quad (17)$$

$$d_c = \frac{3Duz^+z^-}{2(Du + t^+)(z^+ + z^-)} \frac{eE_0 a^3}{kT} \quad (18)$$

where $t^+$is the transport number of counterions defined as:

$$t^+ = \frac{z^+D^+}{z^+D^+ + z^-D^-} \quad (19)$$

The field induced concentration polarization outside the particle's EDL gives rise to conductivity gradient proportional to electrolyte concentration determined as:

$$K_m = \frac{K_{m0}}{c_0}(c_0 + \frac{d_c}{r^2} cos\theta) \quad (20)$$

The non-linear current density arises due to the action of the electric field on K_m:

$$\delta i_2 = -\nabla K_m \frac{K_{m0}}{c_0} \frac{d_c}{r^2} \, cos\theta \quad (21)$$

As can be seen from Fig.6 the conductivity variation is negative at the left hemisphere and positive at the right one, so the radial component of δi_2 is directed outward from the particle at all points of any spherical surface concentric with particle. Consequently, the volume surrounded by this surface will acquire a negative charge. This charge can be found using the fact that the current flowing

out of a spherical surface created by charge δq_2 should compensate the flow related to the currentδi_2:

$$q_2(r) = -\varepsilon_m \oiint_{S_r} \delta i_2 \,.\, \mathrm{dS} = \\ 2\pi\varepsilon_m r^2 \int_0^{\pi} \delta i_{2r}(r) sin\theta d\theta = -\frac{4\pi\varepsilon_m d_c (d_\varphi + E_0 r^3)}{3c_0 r^3} \tag{22}$$

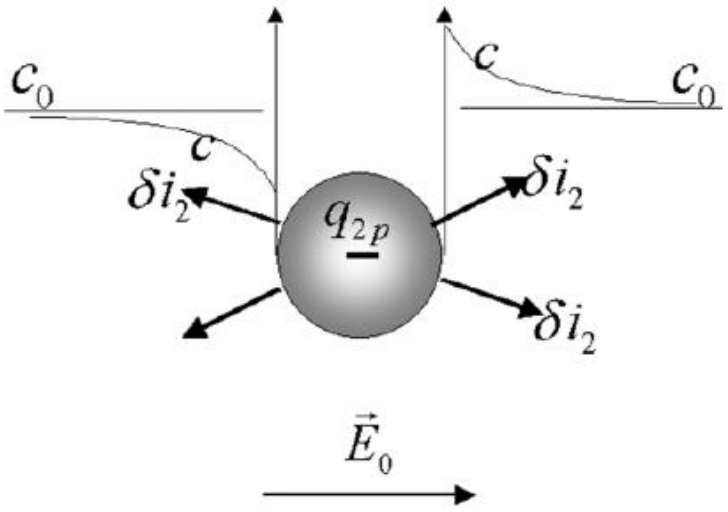

Figure 6. Space- and field- dependent distributions of the conductivity and nonlinear current density component, $\boldsymbol{\delta i_2}$ outside the particle with negative equilibrium charge and field-induced total negative charge $\boldsymbol{q_2}$ of particle together with its EDL [34]

The field induced charge density may be found as:

$$\rho_2(r) = \frac{1}{4\pi r^2}\frac{dq_2(r)}{dr} \tag{23}$$

The bulk electric force can be determined by the action of electric field on the distributed charge density as:

$$f(r,\theta) = -\rho_2(r)\nabla\varphi \tag{24}$$

Navier-Stokes equation for the problem of particle motion consists of continuity and momentum equations as:

$$\nabla.v = 0 \tag{25}$$

$$\eta\nabla^2 v = \nabla P - f(r,\theta) \tag{26}$$

Solution of the Navier-Stokes equations, considering Eq. (23) and (24) with appropriate boundary conditions and approximations leads to the following expression for the cubic electrophoresis:

$$v_{ep}^{(3)} = -\frac{\varepsilon_m}{\eta}\frac{d_c(-4d_\varphi^2 + 63a^3E_0d_\varphi + 42a^6E_0^2)}{189c_0a^7} \tag{27}$$

Substitution of Eqs. (17) and (18) for the dipole moments , yields the final form for the cubic electrophoretic mobility [5]:

$$\mu_{ep}^{(3)} = -a^2\frac{e}{kT}\frac{\varepsilon_m}{\eta}\frac{Du[23 + Du(269 + 464Du)]}{252(1+2Du)^3} \tag{28}$$

In deriving the above expression for the nonlinear electrophoretic mobility, it was assumed that the surface conductivity plays a great role and it is governed by not only the mobile part of the EDL, but also the immobile part [34]. If the

electrokinetic and stern potentials coincide with one other [3, 4], Eq. (28) reduces to:

$$\mu_{ep}^{(3)} = 0.3\frac{e}{kT}\frac{\varepsilon_m}{\eta}\frac{sinh\,(\zeta_0/2)}{\kappa a}a^2 \qquad (29)$$

The total electrophoresis can be described as the sum of the linear and cubic terms[7, 21]:

$$v_{ep} = \mu_{ep}^{(1)}E_0 + \mu_{ep}^{(3)}E_0^3 \qquad (30)$$

Cubic dependence is irrelevant to our experimental data as the Peclet numbers are much higher than unity.

2.2. Nonlinear electrophoresis at large Peclet numbers

In this regime, the concentration field arising outside DL is estimated under the influence of diffusion and convection. The DL deviates strongly from spherical symmetry and electroneutrality, and the screening of the surface charge is provided not only by the diffuse layer but also by the charge induced in the convection-diffusion layer beyond it. Nonlinear electrophoresis at large Peclet numbers was previously considered for two limiting cases of weak and strong concentration polarization. In these limiting cases, the electrolyte concentration along the boundary between diffuse and diffusion layers on the particle side that accepts counterions decrease by 20%-30% or drop to almost zero respectively. The theory developed below uses the approximation of thin DL and CDL:

$$\kappa^{-1} \ll \delta \ll a \tag{31}$$

The condition of a relatively small concentration drop within the limits of diffusion layer implies:

$$|c(r,\theta) - c_0| \ll c_0 \tag{32}$$

At large Peclet numbers, instead of the Laplace equation for the distribution of ion concentration, a more general convection diffusion equation can be solved as follows:

$$D_{\text{eff}}\left(\frac{\partial c(r,\theta)}{\partial r} + \frac{2}{r}\frac{\partial c(r,\theta)}{\partial r}\right) = u_r(r,\theta)\frac{\partial c(r,\theta)}{\partial r} + \frac{u_\theta(r,\theta)\partial c(r,\theta)}{\partial r} \tag{33}$$

where $u_r(r,\theta)$and $u_\theta(r,\theta)$ are the radial and tangential components of the fluid electroosmotic velocity along the thin diffuse layer. By substituting the fluid velocity along the diffusion layer into Eq. 33 we obtain:

$$u_\theta = \frac{\varepsilon\zeta E sin(\theta)}{\eta}, \qquad u_r = \frac{2r}{a}\frac{\varepsilon\zeta E cos(\theta)}{\eta} \tag{34}$$

This also simplifies the form of the boundary condition (10):

$$\frac{\partial c}{\partial r} = \frac{6c_0}{\kappa a}\left(1 + 3msinh\left(\frac{\tilde{\zeta}}{2}\right) + \zeta\right)\tilde{E}\cos(\theta) \tag{35}$$

where

$$m = \frac{2\epsilon}{3\eta D_{eff}}\left(\frac{RT}{F}\right)^2; \tilde{\zeta} = \frac{e\zeta}{kT};\ \tilde{E} = \frac{FEa}{RT} \tag{36}$$

The distribution of velocities (34) also applies near the surface of the floating bubble. In this case the surface of the bubble is mobile and the angular distribution of velocities is described by Eq. (34). A similar angular relationship holds for rather big bubbles with a potential hydrodynamic field. In this case

when a surface-active substance is dissolved in a sufficiently small concentration so as not to have affected the movement of the surface, the process of stationary exchange between the adsorption layer and the bulk is described by a boundary condition similar to (35). Thus, the structures of diffusion layers formed near the dynamic adsorption layer of the bubble and in the electrophoresis at large Peclet numbers are identical if condition (32) is fulfilled in both cases. This allows the immediate use of the initial solution obtained in the theory of the Dorn effect at large Peclet numbers [35] and used repeatedly in the theory of the Marangoni-Gibbs effect [36]

$$\Delta\tilde{c}(\theta,\tilde{r}) = \frac{c_0 - c(\theta,\tilde{r})}{c_0} =$$

$$6Du^*\tilde{E}\left(\frac{1}{4\pi Pe}\right)^{1/2}\int_0^{\theta}\frac{exp\left(-\tilde{r}^2 Pe\, sin^4\theta/4\chi(\theta,\theta\prime)\right)}{\chi^{\frac{1}{2}}(\theta,\theta\prime)}d\theta \qquad (37)$$

where

$$Du^* = \frac{\sinh(\psi_d/2)\left(1+3m+\tilde{\zeta}\right)}{\kappa a};\ \chi(\theta,\theta') = \cos\theta' - \cos\theta - \frac{\cos^3\theta' - \cos^3\theta}{3} \qquad (38)$$

According to [37] the potential drop over the diffusion layer equals to:

$$\psi_d(\theta) = \frac{RT}{F}\frac{D^+ - D^-}{D^+ + D^-}\ ln\left(\frac{c(\theta)}{c_0}\right) \qquad (39)$$

In regime of weak concentration polarization (32) the addition of Smoluchowski and secondary electroosmosis can be assumed. This addition means that the effect of outer field on the charges of diffuse and diffusion layers results in slip velocity expressed by the sum:

$$v^{eo}(\theta) = -\frac{\epsilon E}{\eta}\left(\zeta + \psi_d(\theta)\right) \tag{40}$$

On the basis of Eq. (40) and (37), the velocity distribution of the electroosmotic slip along DL of the particle subject to weak concentration polarization can be calculated. This distribution of electroosmotic velocity allows us to find the change of electrophoresis caused by concentration polarization. For this purpose we can use the expression obtained in [37]:

$$\Delta v_{ep} = \frac{2}{3}\int_0^x \frac{\varepsilon\zeta_1(\theta)}{\eta} E \sin\theta d\theta \tag{41}$$

where

$$\zeta_1(\theta) = \zeta(c(\theta)) - \zeta_0; \zeta_0 = \zeta(c_0) \tag{42}$$

Then the total electrophoresis velocity is equal to:

$$v_{ep} = -\frac{\varepsilon}{\eta}\zeta_0\left(E + \beta E^{\frac{3}{2}}\right) \tag{43}$$

where

$$\beta = \frac{1.66\sqrt{Fa/RT}}{\sqrt{\frac{2}{3}\pi m\left|\tilde{\zeta}_0\right|^{3/2}}} Du\left[\frac{2\,tanh\left(\frac{\tilde{\psi}_d}{4}\right)e^{-\kappa h}}{1 - tanh^2\left(\frac{\tilde{\psi}_d}{4}\right)e^{-2\kappa h}}\left\{\frac{1}{cosh\left(\frac{\tilde{\psi}_d}{4}\right)} + \kappa h\right\} + \frac{\tilde{\zeta}_0}{\left|\tilde{\zeta}_0\right|}\frac{D^+ - D^-}{D^+ + D^-}\right] \tag{44}$$

where Du is defined here as:

$$Du = \frac{2\mu\left(cosh\left(\frac{\tilde{\psi}_d}{4}\right) - cosh\left(\frac{\tilde{\zeta}_0}{2}\right)\right) + 4\,sinh^2\left(\frac{\tilde{\zeta}_0}{4}\right)(1+3m)}{\kappa a} \tag{45}$$

The first five points of our measured data can be considered to fall in the regime of weak concentration polarization as they seem to be consistent with the $E^{3/2}$ dependence.

In the case of strong concentration polarization, condition (32) does not hold. Because of the complexity of the problem in question in this regime, the analytical solution was only obtained for the velocity of electroosmosis [7], [8], [19]. Electric current continuity equation can be expressed as:

$$\nabla.\left[c(r,\theta)\nabla\overline{\psi}(r,\theta)\right]=0 \tag{46}$$

where

$$\overline{\psi}(r,\theta)=F\left[\frac{F}{RT}(D^{+}+D^{-})\phi(r,\theta)+(D^{+}-D^{-})ln\frac{c(r,\theta)}{c_0}\right] \tag{47}$$

We can then find the distribution of potential by solving (47) with respect to concentration distribution:

$$\phi(r,\theta)=\frac{RT}{F^2}\frac{\overline{\psi}(r,\theta)}{(D^{+}+D^{-})}+\frac{RT}{F}\frac{(D^{+}-D^{-})}{(D^{+}+D^{-})}ln\frac{c(r,\theta)}{c_0} \tag{48}$$

The convective diffusion equation can be solved by introduction of a new independent variable known as current function:

$$V_\theta=\frac{1}{r\sin\theta}\frac{\partial\psi}{\partial r};V_r=\frac{1}{r^2\sin\theta}\frac{\partial\psi}{\partial\theta} \tag{49}$$

To eliminate the variable coefficient, we introduce the following new variable in place of θ:

$$t = \int_0^{\theta} \tilde{V}(\theta) \sin^2 \theta d\theta \tag{50}$$

As a result of using these independent variables, the convection diffusion equation is reduced to a more convenient form:

$$\frac{\partial \tilde{c}}{\partial t} = Pe^{-1} a^2 \frac{\partial^2 \tilde{c}}{\partial \psi^2} \tag{51}$$

The boundary condition (10), using the variable ψ, and t takes the form

$$\frac{\partial \tilde{c}}{\partial \psi} = \frac{1}{a} \frac{\partial}{\partial t} \left(\frac{3}{2} \tilde{E} Du^* \sin^2 \theta \right) \tag{52}$$

where

$$Du^* = \frac{2\left(\sinh\left(\tilde{\zeta}_0/2\right)(1+3m)+2m\tilde{\zeta}_0\right)}{\kappa a} \tag{53}$$

Solving (51) subject to (52) under appropriate approximation, the velocity of electroosmotic sleep increases by an amount proportional to E^2as:

$$v_{eo}(\theta) = \frac{\varepsilon}{\eta} \frac{9\pi}{4m} (Du^*)^2 a E^2 \sin\theta \cos\theta \tag{54}$$

According to numerical computation in [8] with respect to Eq. (54), electrophoretic velocity of the particle increases with electric field strength somewhat more slowly than $E^{3/2}$. Our higher velocities may correspond to strong concentration polarization at high Peclet numbers as the data is not completely linear, but still increase slower that $E^{3/2}$ with electric field.

3. Experimental procedure

4.1. Methodology

The experiments were conducted using the simple method [23, 24] of simultaneous measurement of both the fluid and particle velocities in open end capillaries. Following the application of a DC field, the electroosmotic generated in the capillary causes a net motion of the liquid meniscus in the calibrated reservoir from which the flow rate can be calculated. Average electroosmotic velocity then can be computed as:

$$V_{EOS} = \frac{dQ}{dtA_C} \tag{55}$$

Where Q is the volumetric flow rate, and A_c is the cross section of the capillary. Simultaneously, the absolute velocity of the particles along the length of the capillary is measured by tracking their motion in the field of view of a microscope. Once V_{EOS}, and V_{abs} are available, the electrophoretic particle velocity is calculated from their difference,

$$V_{ep} = V_{EOS} - V_{EP} \tag{56}$$

This is true in case the pressure required for maintaining the flow rate is small enough not to generate a significant pressure driven backflow inside the capillary. Using Poiseuille equation in a rectangular channel, we obtain for the average pressure flow:

$$V_{avg} = -\frac{h^2}{8\eta}\frac{dP}{dx} \tag{57}$$

where h is the height of the channel, μ is the fluid dynamic viscosity, and $\frac{dP}{dx}$ is the pressure difference along the channel which in our case coincides with the pressure head in the reservoirs. This yields an average Poiseuille velocity of orders of millimeter per second which is absolutely negligible compared to electroosmosis in our experiments of high electric fields.

4.2. Optical System

The setup shown in figure 7 was used to simultaneously measure particle and flow velocities. The system uses an epi-fluorescence microscope (Model ECLIPSE E600FN, Nikon) with a 60x (NA=1.25) water immersed objective lens. A PI-MAX 3 ICCD camera (1024 x 1024 pixels with 12.8x12.8 µm pixel size) was used to capture the particle images. The light source is a pulsed Nd-YAG laser (Pegasus, New Wave Research) synchronized with ICCD camera and the voltage generator. The light passes through an optical filter cube with a dichroic mirror to reach the microfluidic device. A 11 MP camera is aligned with the micro channel reservoirs to record the displacement of the fluid, simultaneously with µPIV measurements.

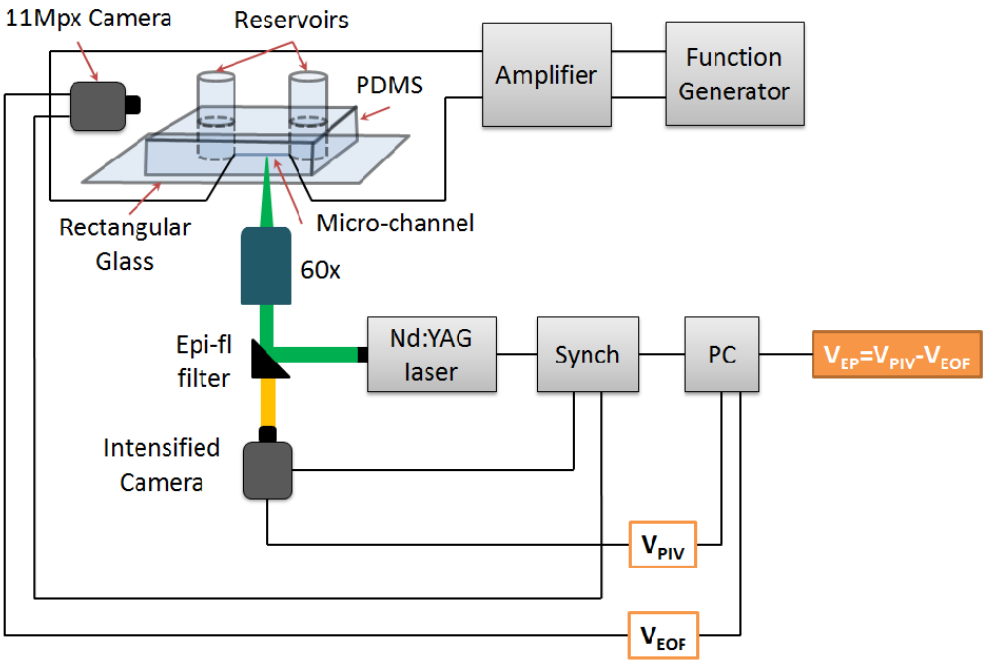

Figure 7. Schematic of the setup for simultaneous particle and flow velocity measurements

4.3. Channel and Suspension Preparation

The fluorescently-dyed particles suspended in the working solution are excited by the light and the emitted fluorescent light is captured by the intensified camera. We used very dilute suspensions of polystyrene spheres (particle diameter $D = 200\ nm$, Duke Scientific Corp). in deionized water. The surface of the particles are treated with carboxyl groups which gets negatively charged when dispersed in aqueous solutions The suspensions were prepared by dispersing $10\ \mu l$ of a 1% (v/v) stock suspension in 50 ml of deionized water. This yields a much diluted suspension with dispersed particles not chaining to or screening each other at very large applied electric fields.

Rectangular polydimethylsiloxane (PDMS) channels with 50x25 μm cross section and 200 μm long were used in the experiments. Using an oxygen plasma treatment, the channels were bonded to a microscope glass cover. Then the channels are connected to graded syringes with an open tip to the atmosphere as reservoirs. Both glass and PDMS surfaces of the channels gain negative charge when in contact with deionized water. Before the measurements, the micro-channels were rinsed with de-ionized water for 20 minutes, then cleaned using 0.1 M NaOH and deionized water for 20 minutes each, and rinsed again with the working solution for 40 minutes.

4.4. Measuring procedures

First, the microchannel reservoirs are filled with the suspension to the same height in order to avoid inducing pressure flow. Once the suspension was filled, the setup is fixed onto the stage of the microscope equipped with the ICCD camera connected to a computer. Platinum electrodes are inserted into the reservoirs and connected to an amplifier synchronized with the voltage generator and ICCD and 11 MP cameras. Once the voltage generator is started, the electrodes are energized via the voltage amplifier; the movement of the particles is recorded by ICCD camera synched with the laser pulses. The imaging plane is at the bottom of the micro-channel near the glass slide. At the same time the displacement of the fluid meniscus in the calibrated reservoir is captured by 11 MP camera. For the lower range of electric fields (Figure 3) DC voltages between 100-1000 V with steps of 200V are applied. For the higher range the voltages between 1000-5000 with steps of 500V are applied.

To avoid undesired effects such as electrolysis, bubble generation and joule heating the measurement time was kept below 1 minute. Following each step, the microchannel was flushed with DI water, and new suspension was filled to reservoirs to prohibit the possibility of salt contaminants in DI water, and the generation of PH gradients associated with gasses dissolved in the suspension from air. Moreover, to estimate the contribution of the possible change in electroosmosis velocity of DI water due to the presence of particles, each step is repeated without particles and just with DI water for further comparison. Each

step is repeated 5 times in different channels in order to ensure the accuracy and reproducibility of the measurements.

The obtained PIV images are analyzed to measure the instantaneous velocity vector fields. Displacements of at least 20 particle images are spatially averaged to obtain the characteristic velocity of the particles for each voltage step. Meniscus displacement and the measurement duration are also averaged over 5 frames to obtain the flow rate in each step.

4. Results and Discussion

When the electric field was applied both the particles and fluid move towards the grounded electrode. Figure 8 depicts electroosmotic velocities for all voltages obtained from flow rate measurements. As mentioned earlier electroosmotic velocities were calculated from the slope of the fluid volume collected in the reservoir as a function of time. The dependence on electric field seems somewhat linear for all the ranges (intermediate and high electric field). Linearity of electroosmosis generally indicates that the symmetry of the EDL and distribution of zeta potential along the microchannel walls remains undisturbed in spite of high electric fields. Smoluchowski dependence according to theoretical values of wall zeta potential in DI water is also illustrated for reference. in DI water The smallest applied electric field is five times larger than previous experiments [2, 10, 13, 18, 25] which used electric fields up to 1000 V/cm to generate a maximum electroosmosis of 5 mm/sec . Figure 8 shows a maximum velocity about 4 m/sec which is two orders of magnitude higher than any electroosmosis measured before. Such large flow rates can be utilized to develop efficient and low cost

micro pumps as well as competitive and miniaturized propulsion technologies. Moreover the fast electroosmosis provides a promising and novel way to manipulate local flow field and enhance mixing in microchannels.

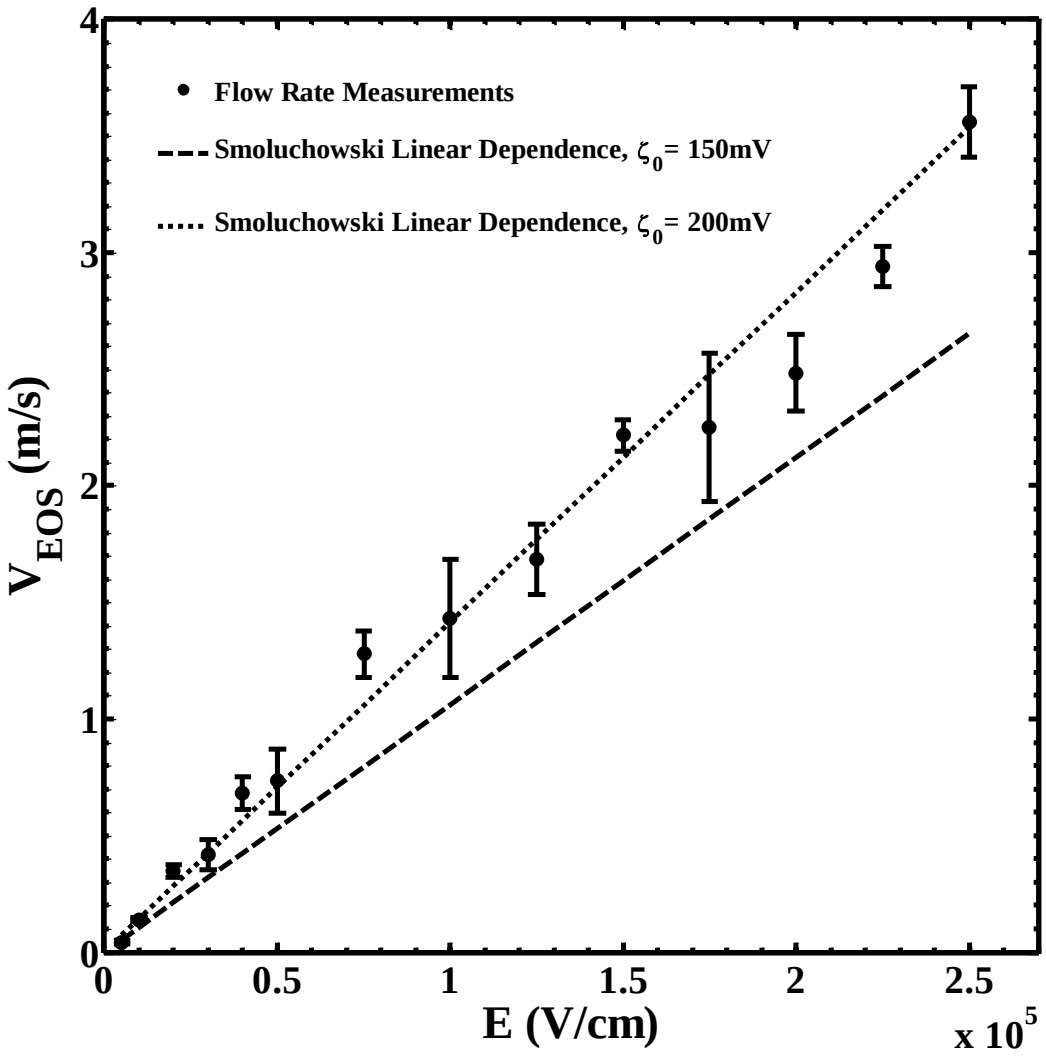

Figure 8. Electroosmotic velocity for all voltages obtained from flow rate measurements. Theoretical curves are calculated according Eq.1 at $\zeta_0 = 150, 200\text{mV}$.

In the classical theory of electrophoresis [1, 2] the electrophoretic mobility of a particle with a thin double layer is a material constant, given by the Smoluchowski formula. In particular, the electrophoretic mobility does not depend on the background field or the shape or size of the particle. These are partly consequences of the assumption of fixed surface charge, or constant zeta potential. For large electric fields however, these assumptions must be modified and the asymmetry in potential distribution in polar direction around the particle should be taken into account. Fig 9.b shows the electrophoretic velocity obtained from our PIV measurements in the range of intermediate voltages. Experimental data obtained in the previous studies are also presented there considering the fact that since large electric field electrophoresis depends on the particle dimension, a proper comparison of electrophoresis among particles of different sizes is not possible. Stepwise electric pulse method was applied to latex particles [3] of different sizes to obtain experimental data 1, and 2 in Fig 9.a. They are in good agreement with theoretical curves 6, and 7 calculated according to Eqs. 29 and 30 which validates the cubic dependence at low Peclet numbers. As the electric field enhances, larger Peclet numbers are gained, therefore in Fig 9.b experimental data 2 and 3 obtained in this regime [14] demonstrate the dependence of electric field strength close to $E^{3/2}$, i.e., theoretical curves 2 and 3 computed based on Eqs. 43 and 44 are consistent with them. Yet, in spite of quite high voltage, due to low surface potential of latex particles, the order of magnitude of the nonlinear electrophoresis velocity remains close to those obtained in data set 2, and 3 in Fig.9a.

As discussed before, earlier studies dealing with strong field electrophoresis did not exceed an applied electric field of 1000 V/cm. Large flow rates in our experiments leads to higher Pe numbers (Pe>10). This range of Peclet number is associated with slower growth of induced space charges and, correspondingly, a slower increase of velocity with applied electric field, compared to classical nonlinear electrophoresis. To our best knowledge, the fastest electrophoretic velocity was reported for pyrite particles of mean diameter of 300 μm, as 20 mm/sec. The maximum velocity in our measurements is about 3 m/sec which is order of magnitude higher than any electrophoresis measured before.

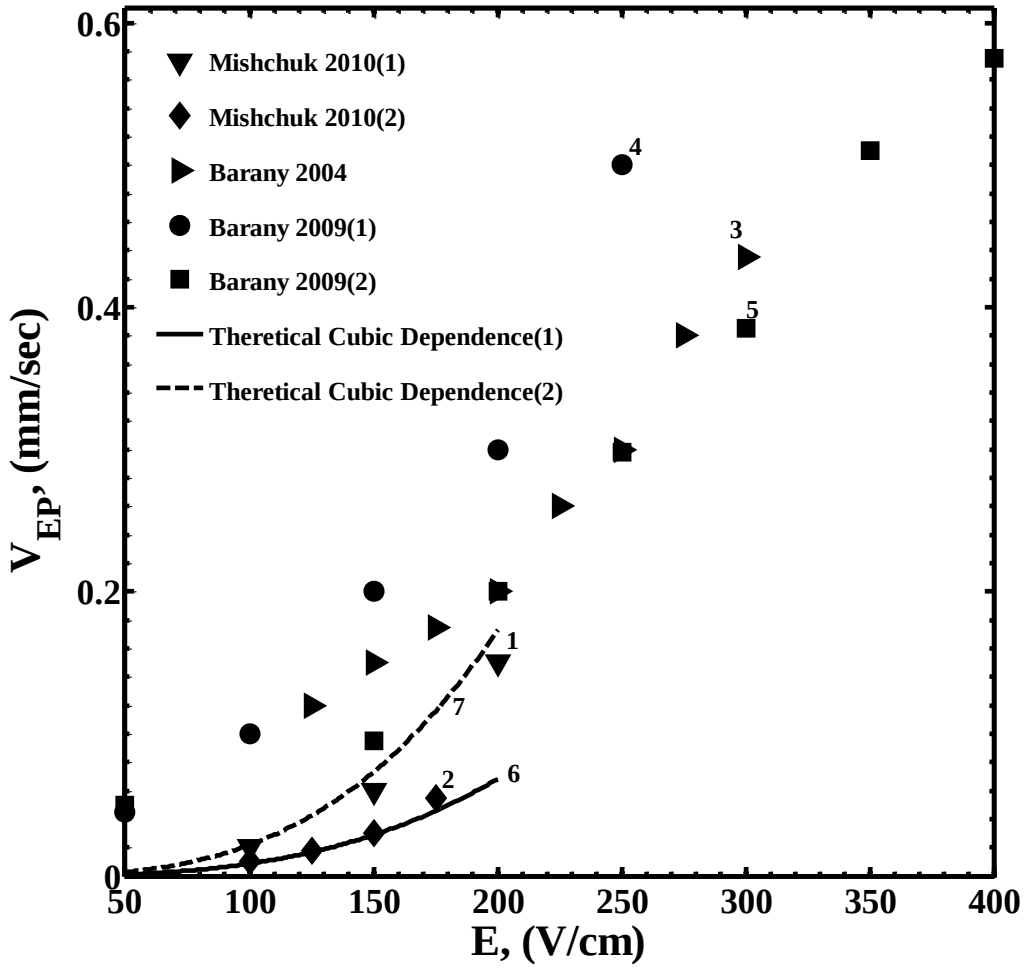
Mishchuk 2010(1)
Mishchuk 2010(2)
Barany 2004
Barany 2009(1)
Barany 2009(2)
Theretical Cubic Dependence(1)
Theretical Cubic Dependence(2)
V_{EP}, (mm/sec)
E, (V/cm)
0
0.2
0.4
0.6
50
100
150
200
250
300
350
400
1
2
3
4
5
6
7

a) $Pe \leq 1$

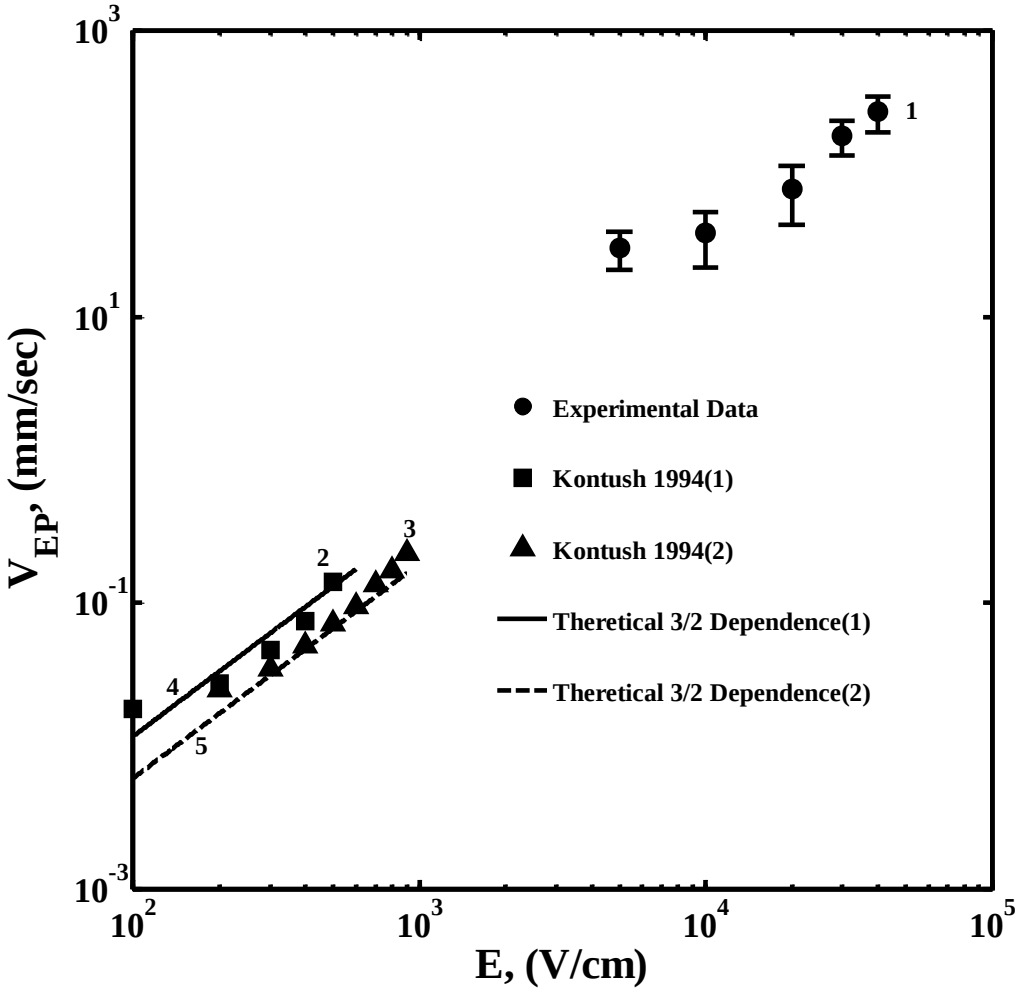

b) Pe $\gg$ **1**

Figure 9. Experimental dependence of electrophoretic velocity on electric field strength at **a)Pe** $\ll$ **1** ; Data set 1, and 2 is adapted from [3] for latex particles $\mathbf{a = 5, 15\mu m}$. Data set 3 obtained from [10] for $\boldsymbol{\gamma - Al_2O_3}$ particles $\mathbf{a = 250\mu m}$. Data set 4, and 5 obtained from [13] for PS particles $\mathbf{a = 30, 50\mu m}$. Curves 9 and 10 theoretical prediction according to Eqs. 29 and 30. **b)Pe** $\gg$ **1** data set 1 is our experimental data; Data set 2, 3 adapted from [14] for latex particles $\mathbf{a = 1.4, 6\mu m}$. Curves 11, and 12 theoretical prediction according to Eqs. 43 and 44.

Fig.10 shows the field dependence of electrophoresis at all ranges. Our experimental data corresponds to curve 1. Curve 2 is calculated according to theoretical linear dependence at an assumed value of $\zeta_0 = 100\text{mV}$. Theoretical curve 3 has been obtained using Eqs.29, and 30. As can be seen from the figure it is clear that it does not match our experimental data which is expected due to our high Peclet numbers, whereas this theory was developed for $Pe \ll 1$. Curve 4 is obtained using Eqs. 43, and 44. This curve somehow is in good agreement with our intermediate electric field data, but it overestimates the data measured at higher electric fields. This trend can be explained by the fact that superfast electroosmosis on the particle surface reduces the thickness of CDL and the corresponding induced space charge layer. The tangential component of the induced potential is no longer negligible which results in the redistribution and shrinkage of the induced space charge. The aforementioned processes result in a slower increase in electrophoresis with respect to applied electric field which makes the trend in Fig.10 to seem almost linear.

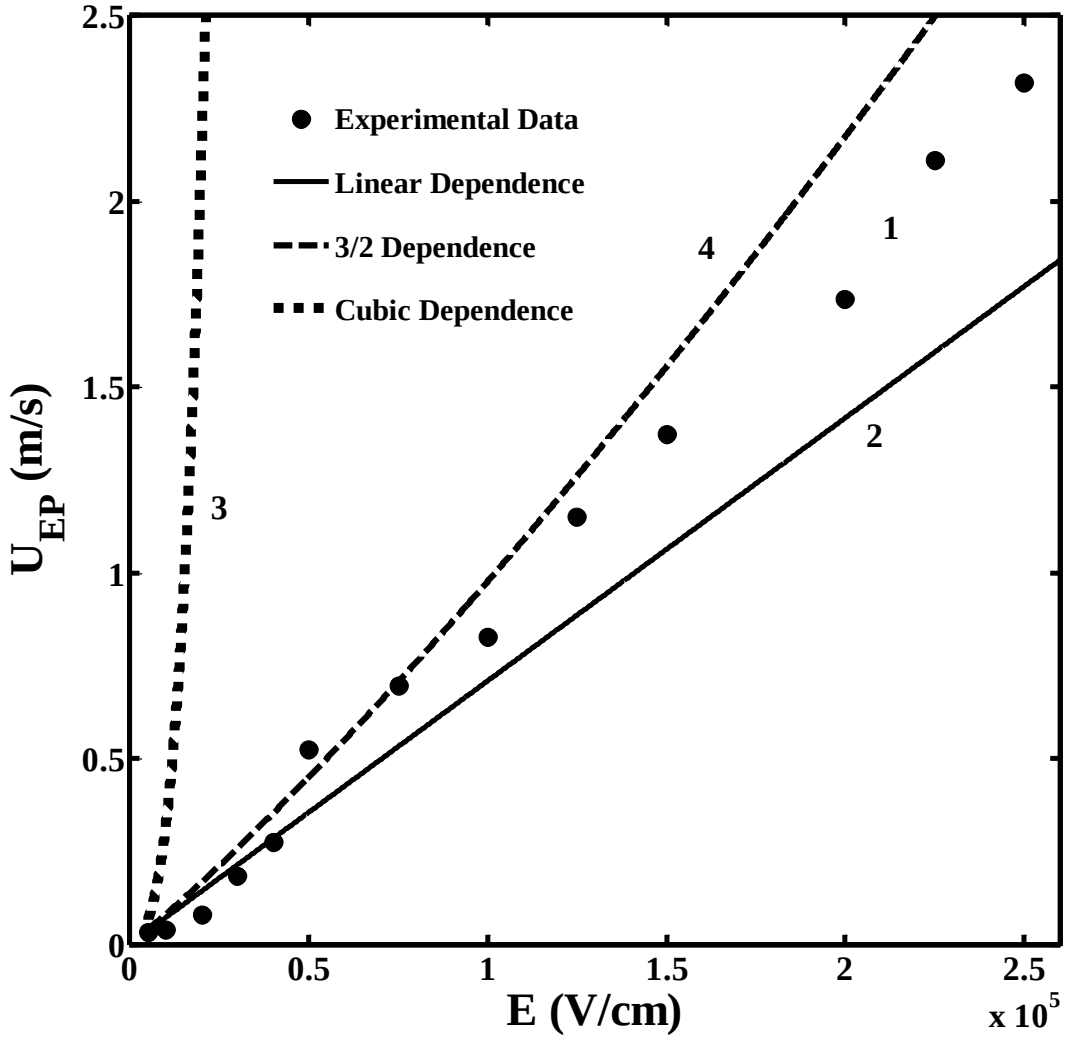

Figure 10. Dependence of electrophoresis on electric field strength (curve 1, experimental data; curve2, 3, and 4 theoretical prediction using $\boldsymbol{\zeta_0 = 100}$mV according to linear dependence Eq.1, cubic dependence, Eqs. 5 and 6, and $\boldsymbol{3/2}$ dependence, Eqs. 7 and 8.

Since our experimental study were not accompanied by further comparison between zeta and stern potentials and finding the electromigration mobility in the immobile part of the EDL, Dukhin number used for obtaining curve 4 was not calculated but fitted using a trial method. Moreover, all nonlinear theories of electrophoresis were developed based on the assumption of a thin double layer:

$$\kappa a \gg 1 \qquad (58)$$

Since the particles used in this study were small, this condition is not fulfilled in DI water where larger thickness of EDL is expected.

It is worth mentioning that a more accurate estimation for electrophoresis is possible by considering the solution to the NS equations and the corresponding slip boundary conditions for the case of non-uniform zeta potential distribution along the walls of a rectangular channel [39]. However, in our calculations the difference in the slip velocities was considered as negligible and the average electroosmotic velocity directly obtained from flow rate measurements was used for evaluation of electrophoresis. This approximation might introduce an error which can be avoided in further studies by repeating the same measurements at the top of the channel on the PDMS side.

5. Conclusion

In this study we measured both the fluid and particle velocities simultaneously in very strong electric fields using PIV and flow rate measurements. Our data were obtained at very large electric fields yielding high Peclet numbers outside the limits of applicability of classical and recently developed theories on nonlinear electrokinetics. Our measurements reveal orders of magnitude higher electrokinetic velocities. These results are critical for designing efficient electrokinetically driven micro pumps as well as employing electrokinetic phenomena in separation, transport, control and manipulation of suspended particles.

6. Bibliography

[1] R. F. Probstein, *Physicochemical hydrodynamics: an introduction*. Wiley-Interscience, 2005.
[2] J. L. Anderson, "Colloid transport by interfacial forces," *Annu. Rev. Fluid Mech.*, vol. 21, no. 1, pp. 61–99, 1989.
[3] N. A. Mishchuk, "Concentration polarization of interface and non-linear electrokinetic phenomena," *Adv. Colloid Interface Sci.*, vol. 160, pp. 16–39, 2010.
[4] S. S. Dukhin and V. N. Shilov, "Kinetic aspects of electrochemistry of disperse systems. part II. induced dipole moment and the non-equilibrium double layer of a colloid particle," *Adv. Colloid Interface Sci.*, vol. 13, no. 1–2, pp. 153–195, 1980.
[5] V. Shilov, S. Barany, C. Grosse, and O. Shramko, "Field-induced disturbance of the double layer electro-neutrality and non-linear electrophoresis," *Adv. Colloid Interface Sci.*, vol. 104, no. 1, pp. 159–173, 2003.
[6] S. S. Dukhin, A. S. Dukhin, and N. A. Mishchuk, "Convective -Diffusion Potential and Secondary Electric Double Layer Under Conditions of Electrophoresis at Large Peclet Numbers," *Colloid J.-Off. Engl. Transl. Kolloidn. Zhurnal*, vol. 50, no. 1, p. 17, 1988.
[7] S. S. Dukhin, "Electrophoresis at large peclet numbers," *Adv. Colloid Interface Sci.*, vol. 36, pp. 219–248, 1991.
[8] N. A. Mishchuk and S. S. Dukhin, "Electrophoresis of Spherical Nonconducting Particles In Strong Concentration Polarization of the Double Layer," *Kolloid Zhurnal*, vol. 50, no. 6, pp. 1111–1118, 1988.
[9] N. A. Mishchuk and S. S. Dukhin, "Electrophoresis of solid particles at large peclet numbers," *Electrophoresis*, vol. 23, no. 13, pp. 2012–2022, 2002.
[10] S. Barany, F. Madai, and V. Shilov, "Study of nonlinear electrophoresis," in *Surface and Colloid Science*, Springer, 2004, pp. 14–20.
[11] S. S. Dukhin, A. K. Vidybida, A. S. Dukhin, and A. A. Serikov, "Aperiodic Electrophoresis. Directed Drift of Dispersed Particles in a Uniform Anharmonic Alternating Electric Field," *Colloid J.*, vol. 49, no. 5, pp. 752–755, 1987.
[12] A. S. Dukhin, "Aperiodic Electrophoresis of Cells," *Colloid J.*, vol. 51, no. 1, pp. 13–18, 1989.
[13] S. Barany, "Electrophoresis in strong electric fields," *Adv. Colloid Interface Sci.*, vol. 147–148, pp. 36–43, Mar. 2009.
[14] S. M. Kontush, S. S. Dukhin, and O. I. Vidov, "Aperiodic Electrophoresis," *Colloid J.-Off. Engl. Transl. Kolloidn. Zhurnal*, vol. 56, no. 5, pp. 579–585, 1994.
[15] N. A. Mishchuk and N. O. Barinova, "Theoretical and experimental study of nonlinear electrophoresis," *Colloid J.*, vol. 73, no. 1, pp. 88–96, Feb. 2011.
[16] S. S. Dukhin, N. A. Mishchuk, and A. A. Rukobratskii, "High-Voltage Pulse Electrophoresis," *Kolloid Zhurnal*, vol. 50, no. 1, pp. 17–24, 1988.
[17] T. S. Simonova and S. S. Dukhin, "Nonlinear Polarization of the diffusion Part of the Thin Double Layer of a Spherical Particle," *Kolloid Zhurnal*, vol. 38, no. 1, pp. 79–85, 1976.
[18] S. S. Dukhin, N. A. Mishchuk, and E. K. Zholkovskii, "Concentration Polarization of the Thin Double Layer of a Spherical Particle at Large Peclet Numbers," *Kolloid Zhurnal*, vol. 49, no. 5, pp. 865–874, 1987.
[19] S. S. Dukhin and N. A. Mishchuk, "Strong Concentration -Polarization of a Thin Double Layer of a Spherical Particle in an External Electric Field," *Colloid J.-Off. Engl. Transl. Kolloidn. Zhurnal*, vol. 50, no. 2, pp. 237–244, 1988.

[20] S. S. Dukhin, “Electrokinetic phenomena of the second kind and their applications,” *Adv. Colloid Interface Sci.*, vol. 35, pp. 173–196, 1991.
[21] T. S. Simonova and S. S. Dukhin, “Nonlinear Electrophoresis of a Dielectric and Conducting Ideally Polarizable Particles,” *Kolloid Zhurnal*, vol. 38, no. 1, pp. 86–93, 1976.
[22] S. S. Dukhin, A. S. Dukhin, and N. A. Mishchuk, “Convective-Diffusion Potential and Secondary Electric Double Layer Under Conditions of Electrophoresis at Large Peclet Numbers,” *Kolloid Zhurnal*, vol. 50, no. 1, pp. 7–16, 1988.
[23] S. S. Dukhin, N. A. Mishchuk, and A. A. Rukobratskii, “High-Voltage Pulse Electrophoresis,” *Kolloid Zhurn*, vol. 50, no. 1, p. 17, 1988.
[24] D. Piwowar, M. E. Tawfik, and F. J. Diez, “High field asymmetric waveform for ultra-enhanced electroosmotic pumping of porous anodic alumina membranes,” *Microfluid. Nanofluidics*, May 2013.
[25] S. S. Dukhin, “Non-equilibrium electric surface phenomena,” *Adv. Colloid Interface Sci.*, vol. 44, pp. 1–134, 1993.
[26] N. A. Mishchuk, “Concentration polarization of interface and non-linear electrokinetic phenomena,” *Adv. Colloid Interface Sci.*, vol. 160, no. 1–2, pp. 16–39, Oct. 2010.
[27] S. S. Dukhin, “Electrochemical characterization of the surface of a small particle and nonequilibrium electric surface phenomena,” *Adv. Colloid Interface Sci.*, vol. 61, pp. 17–49, 1995.
[28] A. V. Delgado, *Interfacial electrokinetics and electrophoresis*. CRC Press, 2001.
[29] N. A. Mishchuk, *Encyclopedia of Surface and Colloid Science*. Marcel Dekker, 2002.
[30] N. A. Mishchuk and P. V. Takhistov, “Electroosmosis of the second kind,” *Colloids Surfaces Physicochem. Eng. Asp.*, vol. 95, no. 2, pp. 119–131, 1995.
[31] N. A. Mishchuk, S. Barany, A. A. Tarovsky, and F. Madai, “Superfast electrophoresis of electron-type conducting particles,” *Colloids Surfaces Physicochem. Eng. Asp.*, vol. 140, no. 1, pp. 43–51, 1998.
[32] N. O. Barinova and N. A. Mishchuk, “Electroosmosis in a system of ionite granules,” *Colloid J.*, vol. 70, no. 6, pp. 690–694, Nov. 2008.
[33] J. Lyklema and M. Minor, “On surface conduction and its role in electrokinetics,” *Colloids Surfaces Physicochem. Eng. Asp.*, vol. 140, no. 1, pp. 33–41, 1998.
[34] V. Shilov, S. Barany, C. Grosse, and O. Shramko, “Field-induced disturbance of the double layer electro-neutrality and non-linear electrophoresis,” *Adv. Colloid Interface Sci.*, vol. 104, no. 1, pp. 159–173, 2003.
[35] S. S. Dukhin, *Kolloid Zhurnal*, vol. 26, pp. 36–44, 1964.
[36] S. S. Dukhin, *Mod. Kapillaritäts-Theor.*, pp. 83–106, 1981.
[37] V. N. Shilov and V. R. Estrela-Lopis, *Surface Phenomena in Thin Films and Disperse Systems*. Nauka, Moscow, 1972.
[38] A. Kumar, E. Elele, M. Yeksel, B. Khusid, Z. Qiu, and A. Acrivos, “Measurements of the fluid and particle mobilities in strong electric fields,” *Phys. Fluids*, vol. 18, no. 12, pp. 123301–1–10, 2006.
[39] S. Devasenathipathy, J. G. Santiago, and K. Takehara, “Particle Tracking Techniques for Electrokinetic Microchannel Flows,” *Anal. Chem.*, vol. 74, no. 15, pp. 3704–3713, 2002.

7. Notation

A_C	Cross section area
a	particle radius
c_0	bulk electrolyte concentration
$c^{\pm}$	Cation and anion concentrations outside DL
D^+	diffusion coefficient of cations
D^-	diffusion coefficient of anions
D_{eff}	effective diffusion coefficient
$D_s^{\pm}$	Surface density of cations and anions
Du	Dukhin number
d_c	Field-induced concentration dipole
d_φ	Field-induced electric dipole
E	Electric field strength
F	Faraday constant
$f(r,\theta)$	Bulk electric force
$I_D^{\pm}$	Component of ion flux caused by diffusion
$I_E^{\pm}$	Component of ion flux caused by electric field
$I_V^{\pm}$	Component of ion flux caused by electroosmosis
$j^{\pm}$	Cation and anion fluxes
h	Height of channel
K^σ	Surface conductivity
K_m	Bulk conductivity

P	Pressure
Pe	Peclet number
Q	Volumetric flow rate
q	Electric charge
R	Gas constant
r	Coordinate counted from the center of particle
T	Temperature
t	time
V_{EOS}	Electroosmosis velocity
V_{ep}	Electrophoresis velocity
δ	Thickness of convective-diffusion layer
ε_0	Vacuum permittivity
ε_r	Relative permittivity
η	Fluid dynamic viscosity
φ	Electric potential
$\Gamma_s^{\pm}$	Surface diffusion coefficient of cations and anions
κ	The reverse of Debye length

$\mu^{\pm}$	Coefficient that describes changes of cation and anion mobility in hydrodynamically immobile part of DL
θ	Angle counted from the direction of external field
$\rho_2(r)$	Field-induced charge density
ψ_d	Stern potential
ζ_0	Electrokinetic potential for linear regime